JOURNAL OF GEOPHYSICAL RESEARCH, VOL. 95, NO. B7, PAGES 11,345–11,358, JULY 10, 1990

Anisotropy in Seismic Velocities and Amplitudes From Multiple Parallel Fractures

LAURA J. PYRAK-NOLTE[1]

Department of Materials Science and Mineral Engineering and Lawrence Berkeley Laboratory Earth Sciences Division, University of California, Berkeley

LARRY R. MYER

Lawrence Berkeley Laboratory, Earth Sciences Division, University of California, Berkeley

NEVILLE G. W. COOK

Department of Materials Science and Mineral Engineering and Lawrence Berkeley Laboratory Earth Sciences Division, University of California, Berkeley

Many rock structures include multiple, near-parallel, planar discontinuities such as bedding planes or joints. The effects of these nonwelded interfaces on seismic wave propagation are often analyzed using effective moduli, in terms of which seismic wave propagation is independent of frequency and without loss, unless the moduli include imaginary terms. An alternative approach is to treat these interfaces as a boundary condition in the seismic wave equation, across which seismic stress is continuous, but seismic particle displacements are discontinuous. The ratio of the stress to displacement is called the specific stiffness of the interface and characterizes the elastic properties of a fracture. For a completely elastic system this results in frequency-dependent reflection and transmission coefficients for each interface as well as a frequency-dependent group time delay. Using multiple, parallel displacement discontinuities and ignoring converted and reflected waves, expressions derived for transmitted wave amplitudes and group velocities show that these depend on frequency, angle of incidence, and polarization in the case of shear waves. Measurements on a laminated steel block show that shear pulses propagating parallel to the laminations and polarized parallel and perpendicular to the plane of the laminations both travel at the velocity for solid steel, although the spectra of these pulses differ considerably. However, the energy of the pulse polarized perpendicular to the laminations may propagate as an interface wave between each pair of laminations. Predictions of the displacement discontinuity model have features quite distinct from many crustal observations to date. We suggest that we are able to model dense populations of coplanar cracks that cannot be treated by effective moduli methods which require a dilute concentration of cracks.

INTRODUCTION

Within the Earth's crust, discontinuities exist that range in size from microcracks to faults and often occur as nearly parallel groups or sets. A set (or sets) of discontinuities, such as fractures, often control the hydraulic and mechanical behavior of a rock mass. Thus determining the location of sets of discontinuities, such as fractures, from seismic information is of great importance to oil recovery from fractured reservoirs, mine stability, waste isolation, and the study of earthquakes.

It is commonly observed that the presence of a set (or sets) of discontinuities results in anisotropy in the material properties of a rock mass. The usual method for calculating the anisotropy in seismic velocities caused by the presence of cracks or fractures is to derive effective elastic moduli for the rock mass. In this method the additional compliance of a dilute population of fractures or cracks is incorporated into an average strain, resulting in effective moduli for the rock as a whole. *Crampin et al.* [1980] calculated the anisotropy in velocity from elastic constants that define a particular anisotropic symmetry. For the purely elastic case, that is, no viscous loss (no complex moduli), the resulting velocities are nondispersive. *Hudson* [1981] investigated the effect of a distribution of a dilute population of cracks or fractures on wave velocities and attenuation. His model assumed that wavelengths were large compared to the size of the cracks and, in an important restriction, that the concentration of cracks was small. Using a static approach to calculate the effect of cracks on the displacement field, elastic constants were derived for a medium containing a set of cracks. From the elastic constants the seismic velocities of the medium containing the cracks were determined. For the case of dry cracks and fractures (no viscous losses), nondispersive wave velocities also result from this formulation. To determine the effect of cracks on attenuation, Hudson also adapted a scattering formulation, using the velocities from the static model. In the model of *White* [1983] the stiffness of individual fractures in a set, as well as their spacing, is incorporated explicitly into expressions for effective moduli. These effective moduli are then used to calculate seismic velocities.

As an alternative to the effective moduli method, an approach which is much more independent of the effective crack density parameter is to treat each fracture or discon-

[1]Now at Department of Earth and Atmospheric Sciences, Purdue University, West Lafayette, Indiana.

Copyright 1990 by the American Geophysical Union.

Paper number 89JB03589.
0148-0227/90/89JB-03589$05.00

tinuity comprised of a population of cracks as a nonwelded interface. The nonwelded interface, which is of zero thickness, is represented by displacement discontinuity boundary conditions in the seismic wave equation. Thus stresses across the interface are continuous, but displacements across the interface are discontinuous. The discontinuity in displacement is equal to the average applied stress divided by the specific stiffness of the interface. Stiffness can, in a qualitative sense, be related to the density of the coplanar cracks. A dense crack population leads to low fracture stiffness, while a dilute crack population leads to a high fracture stiffness. The term "specific stiffness," as opposed to simply "stiffness," is used because specific stiffness has units of stress per unit length, whereas stiffness usually has units of force per unit length. Representing a fracture by such a model yields transmission and reflection coefficients which depend upon the frequency of the seismic wave and upon the ratio of the specific stiffness of the fracture to the seismic impedance of the rock. From the reflection and transmission coefficients a group time delay is found that is a function of the angle of incidence, the frequency of the propagating wave, and the ratio of specific stiffness to seismic impedance.

Several investigators have used the displacement discontinuity boundary conditions to analyze wave propagation through or along nonwelded interfaces. These boundary conditions were used by *Mindlin* [1960] in a study of the coupling between compressional and shear waves at the boundary of elastically restrained, elastic plates. *Kendall and Tabor* [1971] also assumed this boundary condition in their investigation of wave propagation across nonwelded interfaces. The solution for compressional and shear waves propagated at oblique angles of incidence to a displacement discontinuity is given by both *Schoenberg* [1980] and *Kitsunezaki* [1983]. *Schoenberg* [1983] calculated the reflection coefficients for a wave incident on a periodic stratified medium containing displacement discontinuities. From laboratory experiments, *Myer et al.* [1985] showed that the displacement discontinuity model predicted correctly the amplitude behavior of waves propagated across synthetic fractures of calculable stiffness. *Pyrak-Nolte et al.* [1987] formulated an expression for group velocity for waves propagating at normal incidence to fractures and found that the theory correctly predicted experimentally measured values of group velocity from rock samples containing single fractures. For wave propagation along a fracture, *Pyrak-Nolte and Cook* [1987] determined the existence of an elastic interface wave that can travel along a displacement discontinuity and is dispersive. Using both amplitude and velocity data, *Pyrak* [1988] showed that the displacement discontinuity boundary conditions correctly predicted the seismic response of dry natural fractures in rock.

The purpose of this paper is to examine, theoretically, the displacement discontinuity model for wave propagation across a set of plane, parallel fractures. Group velocities and amplitudes for transmitted compressional (P) waves and shear (S) waves are calculated as functions of propagation directions. Group velocities using an effective moduli model are calculated for a transversely isotropic medium composed of parallel fractures for comparison with the results from the displacement discontinuity model. We then present results of laboratory measurements on a laminated block of steel. Group velocities and transmitted wave amplitudes were measured both normal and parallel to the laminae. To relate our work to other available observations, an effective medium model for transverse isotropy developed for thin-bedded sediments was used. Our laboratory data appear to relate to a highly fractured crustal medium that is not often documented but may be of interest to future crustal seismic investigators.

DISPLACEMENT DISCONTINUITY MODEL FOR A FRACTURE

Several investigators have studied the displacement produced by changes in normal and shear stresses across both induced tensile fractures [*Goodman*, 1976; *Swan*, 1983] and natural fractures [*Bandis et al.*, 1983; *Raven and Gale*, 1985]. While it is observed that the displacements in a specimen containing a fracture are greater than those of an intact specimen without a fracture, it is also observed that these additional displacements are concentrated in a region local to the plane containing the fracture. This observation gives rise to the notion that the additional displacements associated with the fracture can be represented as a discontinuity in the displacement field. Experimental observations also show that the fracture deformations are a nonlinear function of stress and that the nonlinearity arises in part because of changes in the geometry of the contact areas as stress on the fracture is increased. The specific stiffness of a fracture under pseudostatic loading is the slope of the tangent to the stress-displacement curve, i.e., it is the ratio of the incremental stress across the fracture to the incremental displacement that the stress produces.

Under dynamic loading, specific stiffness is defined in the same manner as in the pseudostatic case. Intuitively, specific stiffness of the fracture appears to be a relevant parameter that determines the seismic properties of a fracture because it permits a quantitative description of how the mechanical coupling between two fracture surfaces affects wave transmission across the fracture. The main constraint on using the displacement discontinuity model for wave transmission across a single fracture is that the seismic wavelength must be greater than the spacing between the asperites of contact between the two surfaces of the (infinite) planar fracture.

To model wave propagation across a single fracture, we describe the boundary between two elastic, homogeneous isotropic half-spaces as being in nonwelded contact. For the geometry shown in Figure 1 the boundary conditions for an incident compressional plane wave (P wave) impinging on a fracture are

$$u_{z\mathrm{I}} - u_{z\mathrm{II}} = \tau_{zz}/\kappa_z \tag{1}$$

$$u_{x\mathrm{I}} - u_{x\mathrm{II}} = \tau_{zx}/\kappa_x \tag{2}$$

$$\tau_{zz\mathrm{I}} = \tau_{zz\mathrm{II}} \tag{3}$$

$$\tau_{zx\mathrm{I}} = \tau_{zx\mathrm{II}} \tag{4}$$

where

$$\tau_{zz} = \lambda(\partial u_x/\partial x) + (\lambda + 2\mu)(\partial u_z/\partial z) \tag{5}$$

$$\tau_{zx} = \mu[(\partial u_z/\partial x) + (\partial u_x/\partial z)] \tag{6}$$

Seismic stresses are represented by τ; κ_x and κ_z are the specific stiffnesses in the x and z directions, respectively; and u is the seismic particle displacement with subscripts I

and II referring to opposite sides of the fracture. The difference in displacements across the fracture, for example, $u_{zI} - u_{zII}$, is the displacement discontinuity. Equations (1) and (2) require that the magnitude of the displacement discontinuity be equal to the stress divided by the specific stiffness of the fracture. The second boundary condition requires that the stresses across the fracture be continuous. Lame's constants are represented by λ and μ. The same boundary conditions are also applicable for an incident plane *SV* wave (Figure 1).

For an incident plane *SH* wave (Figure 1) the boundary conditions are

$$u_{yI} - u_{yII} = \tau_{zy}/\kappa_y \qquad \tau_{zyI} = \tau_{zyII} \tag{7}$$

where

$$\tau_{zy} = \mu(\partial u_y/\partial z) \tag{8}$$

and fracture stiffness in the y direction is represented by κ_y.

The displacement discontinuity boundary condition does not influence the emergence angles of the reflected and transmitted waves. Only the material properties of the elastic half-spaces affect these angles.

Using solutions which satisfy the wave equation and are of the form

$$u = u_0 \exp(-i\omega t + i\mathbf{k}\cdot\mathbf{X}) \tag{9}$$

where $\mathbf{k}$ is a wave number vector, and $\mathbf{x}$ is a spatial vector, the solution for an incident plane *P* wave, neglecting the time-dependent term, is

$$\begin{bmatrix} -\kappa_z\cos\theta_1 & \kappa_z\sin\phi_1 & -\kappa_z\cos\theta_2 + i\omega Z_{pII}\cos 2\phi_2 & \kappa_z\sin\phi_2 - i\omega Z_{sII}\sin 2\phi_2 \\ -\kappa_x\sin\theta_1 & -\kappa_x\cos\phi_1 & \kappa_x\sin\theta_2 - i\omega(Z_{sII}^2/Z_{pII})\sin 2\theta_2 & \kappa_x\cos\phi_2 - i\omega Z_{sII}\cos 2\phi_2 \\ -Z_{pI}\cos 2\phi_1 & Z_{sI}\sin 2\phi_1 & Z_{pII}\cos 2\phi_2 & -Z_{sII}\sin 2\phi_2 \\ (Z_{sI}^2/Z_{pI})\sin 2\theta_1 & Z_{sI}\cos 2\phi_1 & (Z_{sII}^2/Z_{pII})\sin 2\theta_2 & Z_{sII}\cos 2\phi_2 \end{bmatrix} \cdot \begin{bmatrix} R_p \\ R_s \\ T_p \\ T_s \end{bmatrix} = \begin{bmatrix} -\kappa_z\cos\theta_1 \\ \kappa_x\sin\theta_1 \\ Z_{pI}\cos 2\phi_1 \\ (Z_{sI}^2/Z_{pI})\sin 2\theta_1 \end{bmatrix} \tag{10}$$

The quantity Z is seismic impedance, $Z = \rho V$, where ρ is density, and V is phase velocity. Subscripts I and II refer to the material on either side of the fracture as labeled in Figure 1. The phase velocity is given by $V_p = [(\lambda + 2\mu)/\rho]^{1/2}$ for compressional waves, and $V_s = (\mu/\rho)^{1/2}$ for shear waves. For incident plane *SV* waves the 4 × 4 matrix is the same as for the incident *P* wave, but the product matrix is different:

$$\begin{bmatrix} -\kappa_z\cos\theta_1 & \kappa_z\sin\phi_1 & -\kappa_z\cos\theta_2 + i\omega Z_{pII}\cos 2\phi_2 & \kappa_z\sin\phi_2 - i\omega Z_{sII}\sin 2\phi_2 \\ -\kappa_x\sin\theta_1 & -\kappa_x\cos\phi_1 & \kappa_x\sin\theta_2 - i\omega(Z_{sII}^2/Z_{pII})\sin 2\theta_2 & \kappa_x\cos\phi_2 - i\omega Z_{sII}\cos 2\phi_2 \\ -Z_{pI}\cos 2\phi_1 & z_{s1}\sin 2\phi_1 & Z_{pII}\cos 2\phi_2 & -Z_{sII}\sin 2\phi_2 \\ (Z_{sI}^2/Z_{pI})\sin 2\theta_1 & z_{s1}\cos 2\phi_1 & (Z_{sII}^2/Z_{pII})\sin 2\theta_2 & Z_{sII}\cos 2\phi_2 \end{bmatrix} \cdot \begin{bmatrix} R_p \\ R_s \\ T_p \\ T_s \end{bmatrix} = \begin{bmatrix} +\kappa_z\sin\phi_1 \\ +\kappa_x\cos\phi_1 \\ -Z_{sI}\sin 2\phi_1 \\ +ZsI\cos 2\phi_1 \end{bmatrix} \tag{11}$$

Because incident plane *SH* waves do not generate converted *P* or *SV* waves when impinging on an interface, the solution is reduced to a 2 × 2 matrix:

$$\begin{bmatrix} -\kappa_y & \kappa_y - iZ_{sII}\omega\cos\phi_2 \\ Z_{sI}\cos\phi_1 & Z_{sII}\cos\phi_2 \end{bmatrix} \cdot \begin{bmatrix} R \\ T \end{bmatrix} = \begin{bmatrix} \kappa_y \\ Z_{sI}\cos\phi_1 \end{bmatrix} \tag{12}$$

The sign in front of $i\omega t$ in (9) is arbitrary. Choosing a positive instead of a negative sign would yield solution matrices with signs consistent with those found in texts such as that of *Aki and Richards* [1980].

The transmission coefficient for a *P* wave at normal incidence, with equal material properties on either side of the fracture, is

$$T_p(\omega) = 2(\kappa_z/Z_p)/[-i\omega + 2(\kappa_z/Z_p)] \tag{13}$$

In the limit, as specific stiffness tends to infinity, the solution reverts to the solution for a welded contact, i.e., $T \to 1$ and $R \to 0$. As specific stiffness tends to zero, the solution reverts to the case of a free surface where all of the energy is reflected, i.e., $T \to 0$ and $R \to 1$. In general, this solution has the characteristics of a low pass filter with a cutoff frequency of $2\kappa/Z$. As the specific stiffness of the fracture increases, the cutoff frequency also increases.

The shift in phase of the transmitted wave, Θ_T, caused by the fracture is related to the ratio of the imaginary part of the transmission coefficient to the real part of the transmission coefficient. For normal incidence it is given by

$$\Theta_T = \tan^{-1}[\omega/2(\kappa/Z)] \tag{14}$$

This phase shift is dependent on frequency and the ratio of fracture specific stiffness to seismic impedance.

The group time delay for the transmitted wave is given by

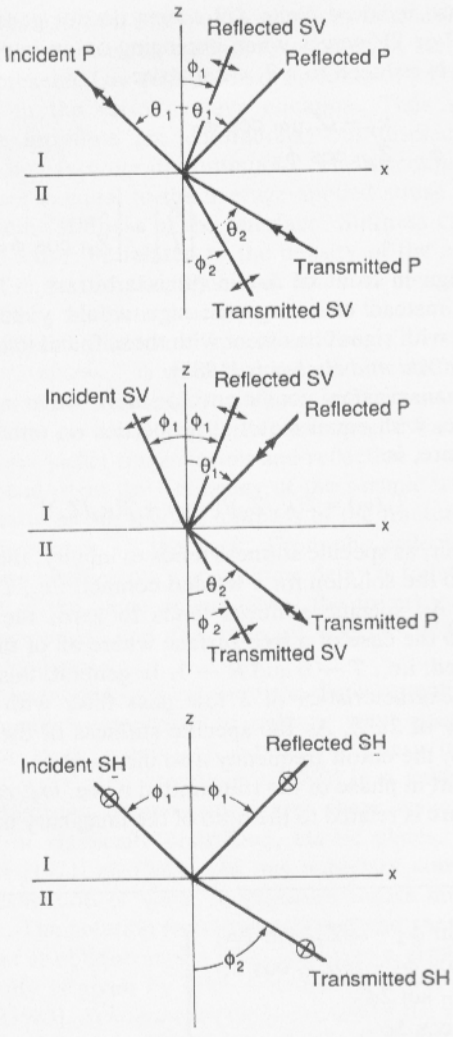

Fig. 1. Coordinate system used in the displacement discontinuity model showing location of fracture and angles of emergence, for incidence P wave, SV wave, and SH wave.

$$t_{gT} = d\Theta_T/d\omega \tag{15}$$

Thus the presence of a fracture causes a delay in the propagating wave front at the fracture. Because the phase shift depends both on frequency and on the specific stiffness, the group time delay for the transmitted wave is also a function of frequency and fracture specific stiffness. For normal incidence,

$$t_{gT} = 2(\kappa/Z)/[4(\kappa/Z)^2 + \omega^2] \tag{16}$$

We have extended this model for a single fracture to calculate the anisotropy in group velocities and amplitudes of seismic waves transmitted at oblique angles across multiple parallel fractures, where the material on either side of the fracture is elastic, homogeneous, and isotropic. Multiple reflections are ignored in order to more clearly demonstrate the characteristic properties of the displacement discontinuity model for the multiple fracture case. We recognize that multiple reflections can have significant effects on the amplitude of the reflected and transmitted waves, particularly in cyclically stratified media. This problem has been addressed by *Schoenberger and Levin* [1974], *Spencer et al.* [1977], *Banik et al.* [1985], and others assuming welded interfaces between layers. We also assume that the specific stiffness of one fracture, and hence its effect on wave propagation, is not a function of the proximity of other fractures. Experimental results by *Hopkins et al.* [1988] indicate this is true as long as fracture spacing is not comparable to the spacing between asperities.

Having made these assumptions, the magnitude of the transmission coefficient for a wave propagating across a set of parallel fractures is simply $|T|^N$, where $|T|$ is the value of the transmission coefficient for a single fracture and N is the number of fractures.

Group time delays of waves at oblique angles of incidence can be calculated from the shift in phase using (15). The solution matrix (equation (10) for P waves, (11) for SV waves, and (12) for SH waves) is solved for the transmission coefficient as a function of angle of incidence. The phase shift is determined from the ratio of the imaginary part of the transmission coefficient to the real part. The group time delay can then be determined from the change in phase with respect to change in frequency. The expression for the group travel time, t_{eff}, for a medium containing a set of N fractures can be obtained from

$$t_{\text{eff}} = (L/U \cos\theta) + Nt_{gT} \tag{17a}$$

where t_{gT} is the group time delay caused by a single fracture (equation (15)), U is the group velocity in intact rock (assuming the intact rock is isotropic and nondispersive so that U is equivalent to the phase velocity V), and L is the total path length along a line normal to the planes. The first term of (17a) is the group time delay caused by the wave traveling through the intact rock, while the second, frequency-dependent term is the group time delay that arises because of the change in the phase across the fractures. As the angle of incidence is increased from 0° to 90°, the path length must increase to intersect the same number of fractures at a certain spacing. To account for this increase in path length, L is divided by cos θ, where θ is the angle of incidence. The resulting effective group velocity

$$U_{\text{eff}} = \frac{L/\cos\theta}{t_{\text{eff}}} \tag{17b}$$

is a function of the frequency of the seismic wave, the angle of incidence, and the ratio of specific stiffness of the fracture to the seismic impedance of the intact rock.

Before discussing results for the general case, it is of interest to look at the effect of a set of fractures upon the group velocity of a normally incident wave. Using the expression for t_{gT} from (16), (17a) becomes

$$t_{\text{effn}} = \frac{L}{U} + N\frac{2(\kappa/Z)}{4(\kappa/Z)^2 + \omega^2} \tag{18}$$

The effective group velocity for normal incidence, U_{effn}, is thus

$$U_{\text{effn}} = \frac{L}{t_{\text{effn}}} = \frac{U\{1 + [\omega/(2\kappa/Z]^2\}}{1 + [\omega/(2\kappa/Z)]^2 + (NUZ/2L\kappa)} \tag{19}$$

Theoretical curves of U_{effn} for compressional waves as a function of frequency are shown in Figure 2, for several values of κ/Z. A constant intact rock impedance (V = 5600 m/s, ρ = 2600 kg/m^3) is assumed, and L/N is set to 0.077 m/fracture. For any value of κ/Z, Figure 2 shows that there

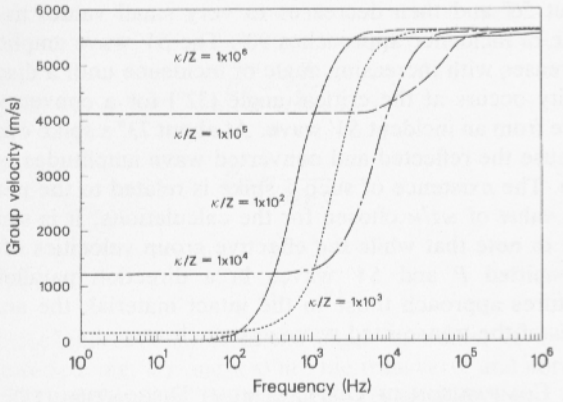

Fig. 2. Group velocity as a function of frequency for a range of (κ/Z) for waves of normal incidence upon a set of fractures.

is a range of low frequencies for which the group velocity is a minimum and changes little with frequency. This is because, as seen from (16), the group time delay is large and approaches a constant when ω is small relative to κ/Z. When ω is large compared to κ/Z, (16) shows that the group time delay approaches zero. Thus the effective group velocities, as shown in Figure 2, approach the group velocity in the intact material at high frequencies. Between these two extremes there is a rapid decrease in the group time delay, resulting in a rapid increase in effective group velocity. The last term in the denominator of (19) includes the stiffness but is independent of the frequency, so that the group velocities in Figure 2 cannot be characterized solely by the dimensionless parameter $\omega = 2\kappa/Z$. Notice that at some frequencies,

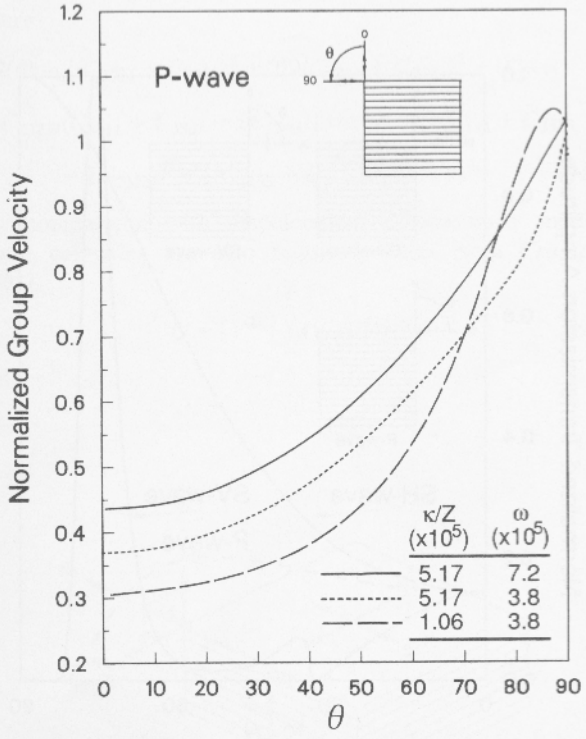

Fig. 3. Normalized P wave group velocity as a function of angle of incidence calculated from the displacement discontinuity model for a fracture spacing of 0.003 m and different values of κ/Z and ω. The inset shows the angle of incidence and the polarization of particle motion.

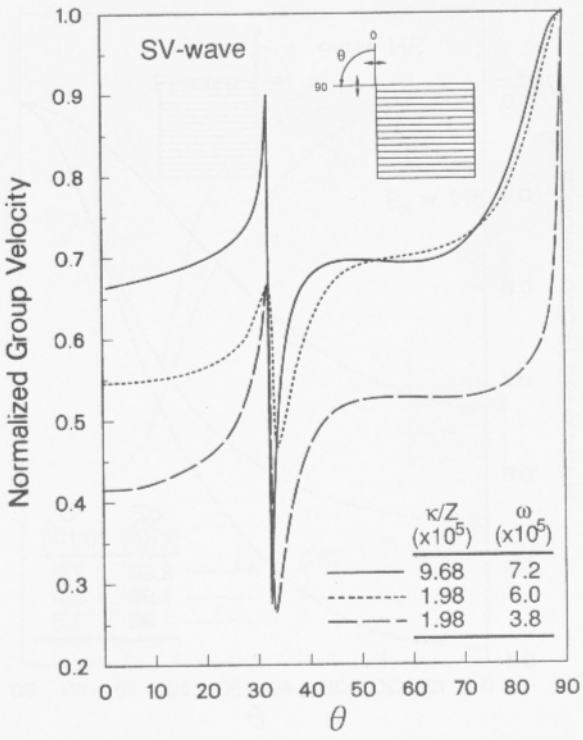

Fig. 4. Normalized SV wave group velocity as a function of angle of incidence calculated from the displacement discontinuity model for a fracture spacing of 0.003 m and different values of κ/Z and ω. The inset shows the angle of incidence and the polarization of particle motion.

fractures of high stiffness will result in a lower effective group velocity (but larger amplitudes) than fractures of lower stiffness. It is also observed that at a particular frequency, different values of κ/Z yield the same group velocity. For example, at a frequency of 1×10^3 Hz the same group velocity is found for $\kappa/Z = 1 \times 10^3\ s^{-1}$ and $1 \times 10^4\ s^{-1}$. The region where the effective group velocity for the fractured rock approaches the group velocity of the intact rock corresponds to the range of frequencies where the transmission coefficient is a minimum and the reflection coefficient is a maximum. In this region, more information about the fractures is contained in the transmission or reflection amplitudes than in the travel times.

The influence of the angle of incidence on the effective group velocities as predicted by the displacement discontinuity model for a set of fractures is shown in Figures 3, 4, and 5. Values plotted in the figures were calculated using (17*a*) and (17*b*) and normalized with respect to the group velocity in intact material. Results in these figures are also for one value of fracture spacing. The selection of this value is arbitrary, but to be consistent with experiments discussed later, a fracture spacing of 0.003 m was assumed. Thus for $L = 1$ m, N equals 333. Calculations were carried out at different values of ω and κ/Z to show the effect of variation in these parameters.

For a transmitted P wave as shown in Figure 3, the displacement discontinuity model predicts that as the angle of incidence increases, the effective group velocity increases and approaches the group velocity of the intact material at an angle of incidence of 90° (parallel to the fractures). Thus the displacement discontinuity theory predicts that when the

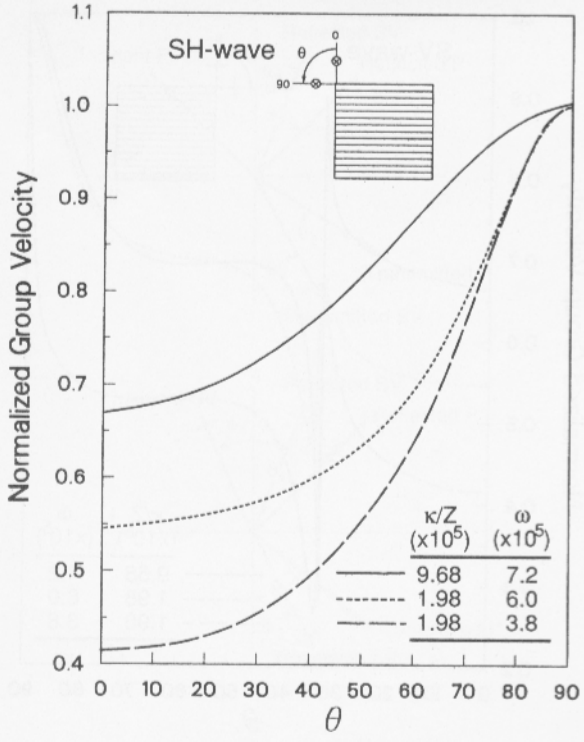

Fig. 5. Normalized *SH* wave group velocity as a function of angle of incidence calculated from the displacement discontinuity model for a fracture spacing of 0.003 m and different values of κ/Z and ω. The inset shows the angle of incidence and the polarization of particle motion.

wave travels parallel to the fracture, the fractures cause no delay in the wave front. The values of one curve in Figure 3 rise slightly above unity at angles of incidence between 80° and 90°. This arises because the group time delay, as calculated from (15), becomes negative. Comparison of the two curves for which κ/z are equal shows that at all angles of incidence, if ω increases while κ/z is held constant, the *P* wave group velocity also increases.

Figures 4 and 5 contain curves of effective group velocities predicted by displacement discontinuity model as functions of the angle of incidence for the two polarizations of shear waves. The effective group velocities predicted by the displacement discontinuity model for an *SV* wave (Figure 4) and an *SH* wave (Figure 5) are equal to one another at both the 0° incidence (perpendicular to the fractures) and 90° incidence (parallel to the fractures). Perpendicular to the fractures, both the *SH* and the *SV* waves are slowed, while parallel to the fractures, neither are slowed. The discontinuity in the *SV* wave effective group velocity corresponds to a critical angle for a converted *P* wave generated by the incident *SV* wave. For a constant value of κ/Z, increasing ω leads to higher group velocities for both shear waves.

In addition to a group time delay the displacement discontinuity model also predicts changes in the amplitudes of the transmitted seismic waves. Figure 6 is a graph showing the effect of 30 fractures on transmitted *P*, *SH*, and *SV* wave amplitudes, for $\omega Z/\kappa = 0.744$, normalized with respect to the amplitudes (assumed equal to 1) of the incident waves. The amplitudes of the transmitted *SH* wave increases with increasing angle of incidence. The transmitted *P* wave amplitude increases with increasing angle of incidence to about 56° and then decreases to very small values as the angle of incidence approaches 90°. The *SV* wave amplitude decreases with increasing angle of incidence until a discontinuity occurs at the critical angle (32°) for a converted *P* wave from an incident *SV* wave. At about 73° a spike occurs because the reflected and converted wave amplitudes go to zero. The existence of such a spike is related to the particular value of $\omega z/\kappa$ chosen for the calculations. It is significant to note that while the effective group velocities of the transmitted *P* and *SV* waves in a direction parallel to fractures approach those in the intact material, the amplitudes of the transmitted wave approach zero.

Comparison of Displacement Discontinuity Model to Effective Moduli Model

In order to compare the two models, expressions for effective moduli which include, explicitly, the properties of the fractures are required. In the effective moduli model a rock mass containing a single set of plane parallel fractures can be represented by a transversely isotropic medium described by five elastic constants. Using an average strain method, *Amadei and Goodman* [1981], *Schoenberg* [1983], *Majer et al.* [1988], and others have derived expressions for the five effective elastic constants in terms of the elastic properties of the intact rock, fracture spacing, and fracture specific stiffness. These elastic constants for the coordinate system shown in Figure 7 are

$$C_{1212} = \mu C_{1111} = [1 + 4(1 - \gamma)E_n]C_{3333}$$
$$C_{1133} = (1 - 2\gamma)C_{3333}$$
$$C_{2323} = \mu/(1 + E_T) = C_{1313}$$
$$C_{3333} = \mu/(\gamma + E_N) \qquad (20)$$

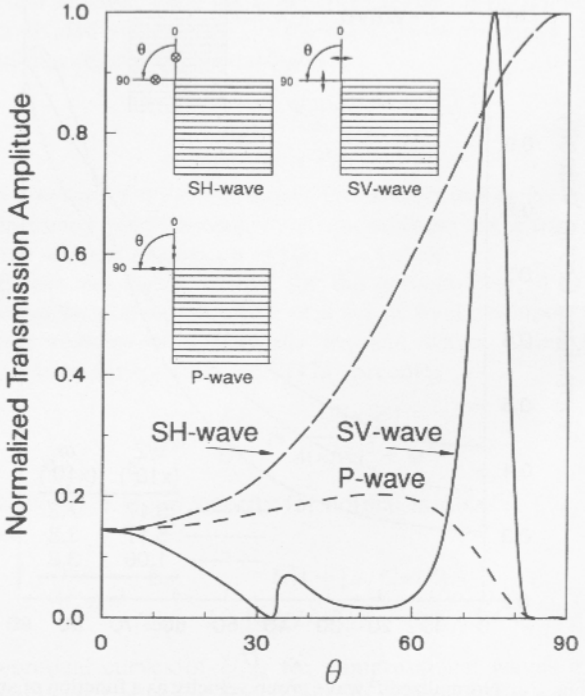

Fig. 6. Effect of 30 fractures on the normalized transmitted amplitude for the case of $\omega Z/\kappa = 0.744$ for *P*, *SV*, and *SH* waves. The inset shows the angle of incidence and the polarization of particle motion.

where

$$E_T = \frac{\mu}{H\kappa_T}$$

$$E_N = \frac{\mu}{H\kappa_N}$$

$$\gamma = \frac{1 - 2\nu}{2(1 - \nu)}$$

In these expressions, μ is the shear modulus; H is the fracture spacing; κ_T and κ_N are the transverse and normal specific stiffnesses of the fractures, respectively; and ν is Poisson's ratio. The ratios E_T and E_N express the contribution of the fractures to the stiffness of the rock mass. As $\kappa \to \infty$, $E \to 0$ and the values of the elastic constants become equal to those of an isotopic elastic medium defined by μ and ν. Hence velocities would be equal to the those of a material containing no fractures.

From *Thomsen* [1986] and others the phase velocity V as a function of the angle of incidence θ, that is, the angle between the direction of propagation of the phase velocity and the normal to the plane of the fractures, can be calculated from the following equations:

$$\rho V_p^2(\theta) = \tfrac{1}{2}[C_{3333} + C_{2323} + (C_{1111} - C_{3333}) \sin^2 \theta + D(\theta)] \quad (21a)$$

$$\rho V_{s2}^2(\theta) = \tfrac{1}{2}[C_{3333} + C_{2323} + (C_{1111} - C_{3333}) \sin^2 \theta - D(\theta)] \quad (21b)$$

$$\rho V_{s1}^2(\theta) = C_{1212} \sin^2 \theta + C_{2323} \cos^2 \theta \quad (21c)$$

where

$$D(\theta) = \{(C_{3333} - C_{2323})^2 + 2[2(C_{1133} + C_{2323})^2 - (C_{3333} - C_{2323})(C_{1111} + C_{3333} - 2C_{2323})] \sin^2 \theta + [(C_{1111} + C_{3333} - 2C_{2323})^2 - 4(C_{1133} + C_{2323})^2] \sin^4 \theta\}^{1/2} \quad (21d)$$

For comparison with displacement discontinuity model, group velocities are also required. Thus from *Crampin* [1981],

$$U = [V^2 + (dV/d\theta)^2]^{1/2} \quad (22)$$

and

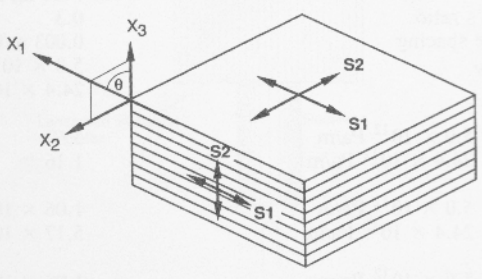

Fig. 7. Coordinate system for effective moduli method showing particle motion of $S1$ wave and $S2$ wave.

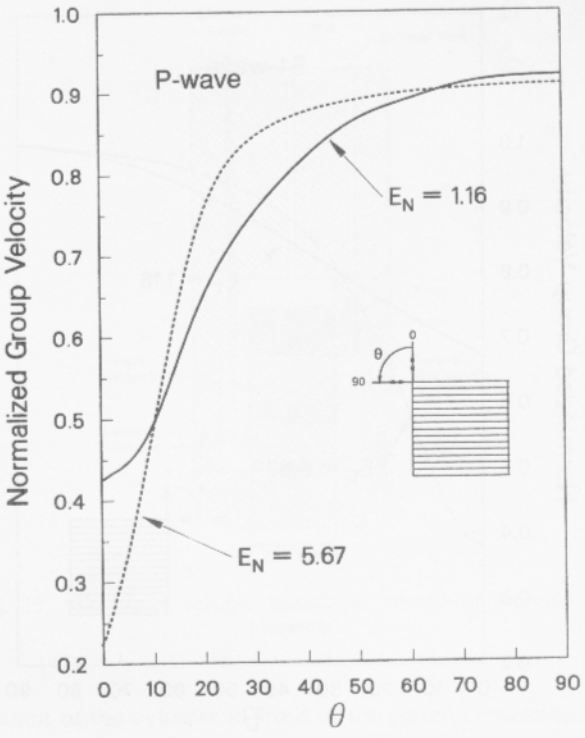

Fig. 8. Normalized P wave group velocity as a function of angle of incidence calculated from the effective moduli method for two different values of E_N. The inset shows the angle of incidence and the polarization of particle media.

$$\Psi = \tan^{-1}\left[\frac{V \sin \theta + \frac{dV}{d\theta} \cos \theta}{V \cos \theta - \frac{dV}{d\theta} \sin \theta}\right] \quad (23)$$

where U is the magnitude of the group velocity; Ψ is the angle between the direction of propagation of the phase and group velocities; and V is the phase velocity in a direction θ, the angle of incidence. The group and phase velocities are equal only for angles of incidence of 0° and 90°.

The angular dependence of group velocities for P, $S1$, and $S2$ waves propagated through a transversely isotropic medium is shown in Figures 8, 9, and 10. The directions of the particle motion with respect to the fractures for $S1$ and $S2$ waves at angles of incidence of 0° and 90° are shown in Figure 7. At 90°, $S2$ wave particle motion is perpendicular to the fractures, and $S1$ wave particle motion is parallel to the fractures.

The values of group velocity shown in Figures 8, 9, and 10 were calculated for material property values and fracture specific stiffness values given in Table 1. To be consistent with the displacement discontinuity model calculations, the material properties of steel and a fracture spacing of 0.003 m were assumed. The table also shows the values of E_N and κ/Z which correspond to the assumed values of fracture specific stiffness.

Figure 8 shows how the group velocity of P waves increases from a minimum at 0° incidence to a maximum at 90°. At 0° incidence the values of group velocity for the medium with fractures of low specific stiffness are, as expected, lower than for the medium with fractures of high

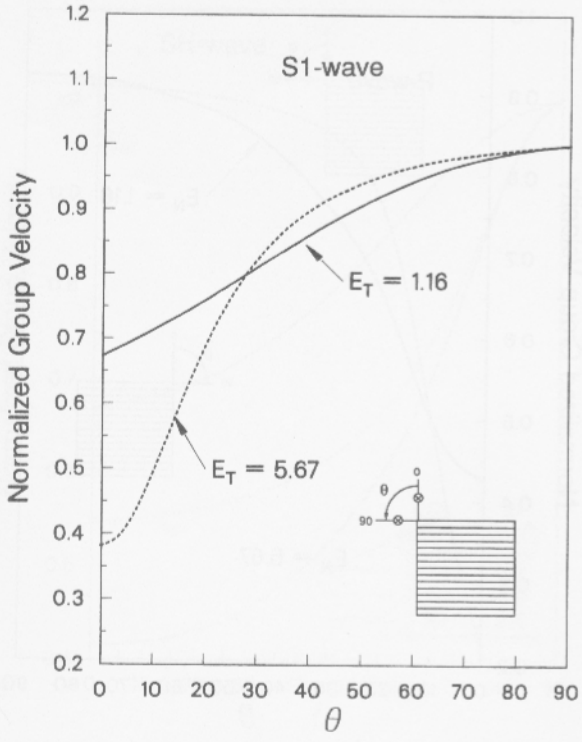

Fig. 9. Normalized $S1$ wave group velocity as a function of angle of incidence calculated from the effective moduli method for two different values of E_T. The inset shows the angle of incidence and the polarization of particle motion.

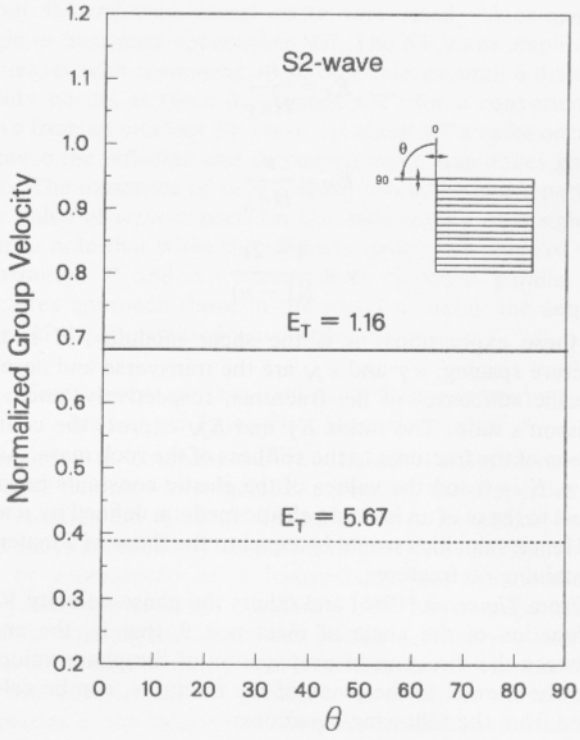

Fig. 10. Normalized $S2$ wave group velocity as a function of angle of incidence calculated from the effective moduli method for two different values of E_T. The inset shows the angle of incidence and the polarization of particle motion.

specific stiffness. However, for the selected material parameters, in the range of about 10°–45°, this trend is reversed. At 90° incidence the group velocity is less than the intact velocity because of the effect of the fractures on the Poisson expansion of the material.

Comparison with the displacement discontinuity model results (Figure 3) shows that for the same value of specific stiffness there are significant differences in the shape of the P wave group velocity curves as a function of angle of incidence. In addition, at 90° incidence, while the effective moduli model predicts a group velocity less than that of intact material, the displacement discontinuity model predicts that the group velocity will equal that of the intact material.

Figure 9 shows that the $S1$ group velocity increases from a minimum at 0° incidence to a value equal to that for intact material at 90° incidence. For S wave particle motion as defined in Figures 1 and 7, it is consistent to compare results of displacement discontinuity model for SH waves (Figure 5) to those for the $S1$ waves. Both models predict that at 90° incidence, with particle motion parallel to the fractures, the shear wave velocity will approach that of the intact material.

For the particular material properties selected, Figure 10 shows that the group velocity predicted by the effective moduli model for an $S2$ wave is less than the value for intact material and is essentially invariant with angle of incidence. As expected, it is equivalent to the $S1$ wave group velocity at 0° incidence. Because of similar particle motions the SV wave group velocities from the displacement discontinuity model (Figure 4) can be compared to the $S2$ wave group velocities from the effective moduli model. Both models predict slowing of the shear wave for propagation perpendicular to the fracture planes. However, for the same values of fracture specific stiffness the variation of group velocity with angle of incidence is completely different for the two models. These differences could have significant implications with respect to interpretation of field vertical seismic profile (VSP) or cross-hole results in which propagation directions vary over a wide range of angles.

In Figure 10 the invariance of the $S2$ wave group velocity with angle of incidence arises from the choice of equal values for E_N and E_T. Selection of values of E_T less than E_N would result in an angular variation such as is more typically expected for a transversely isotropic media. Selection of unequal values of κ_N and κ_T, however, would not substantially change the

TABLE 1. Material Properties and Other Constants Used in Calculation of Group Velocities

Property	Value
Shear modulus	82.15 GPa
Density	7750 kg/m^3
Poisson's ratio	0.3
Fracture spacing	0.003 m/fracture
$\kappa_T = \kappa_N$	5.0×10^{12} Pa/m
	24.4×10^{12} Pa/m
$E_N = E_T$	
$\kappa_N = 5.0 \times 10^{12}$ Pa/m	5.67
$\kappa_N = 24.4 \times 10^{12}$ Pa/m	1.16
κ_N/Z_p	
$\kappa_N = 5.0 \times 10^{12}$ Pa/m	1.06×10^5 s^{-1}
$\kappa_N = 24.4 \times 10^{12}$ Pa/m	5.17×10^5 s^{-1}
κ_T/Z_s	
$\kappa_N = 5.0 \times 10^{12}$ Pa/m	1.98×10^5 s^{-1}
$\kappa_N = 24.4 \times 10^{12}$ Pa/m	9.68×10^5 s^{-1}

general character of the predictions of the displacement discontinuity model. It is also clear from the results that the medium represented by a sequence of layers differs greatly from models of dilute populations of cracks commonly observed in the crust (e.g., papers in this issue). In this sense we suggest that displacement discontinuity models address an entirely different class of crustal fracture sets.

EXPERIMENTAL PROCEDURE

A block of laminated mild steel plates was used to simulate on a laboratory scale the effect of parallel, multiple fractures on the velocities and amplitudes of seismic waves propagated perpendicular and parallel to the fractures. To simulate the surfaces of the fractures, the surfaces of the steel plates were sandblasted before stacking and bolting the plates together. After 31 plates, each 0.00318 m thick, were bolted together to form a block, the outer surfaces were ground flat and parallel. The final dimensions of the block were 0.0906 m perpendicular to the fractures by 0.0905 m parallel to the fractures. For comparisons, measurements were made on a solid steel cylinder that measured 0.0990 m in length by 0.1026 m in diameter.

The steel block was loaded biaxially in a test frame as shown schematically in Figure 11. One actuator was used to clamp the plates together, and the other applied an equal load parallel to the plates. The seismic transducers, one for transmission and the other for reception, were loaded in series with the block to establish seismic coupling.

Each transducer comprises a thick-walled, hardened steel cylinder (Figure 12). One transducer contains the compressional and shear wave piezoelectric elements for transmission, and the other transducer those for reception of the seismic pulses. The end of each transducer in contact with the sample is closed by a thick hardened steel plug with parallel surfaces. The piezoelectric elements and their combined electrodes are stacked sequentially behind each end closure. In back of the electrode is a piston with an *O* ring seal. The space behind this piston is piped to a bottle of high-pressure nitrogen with a pressure regulator, while the

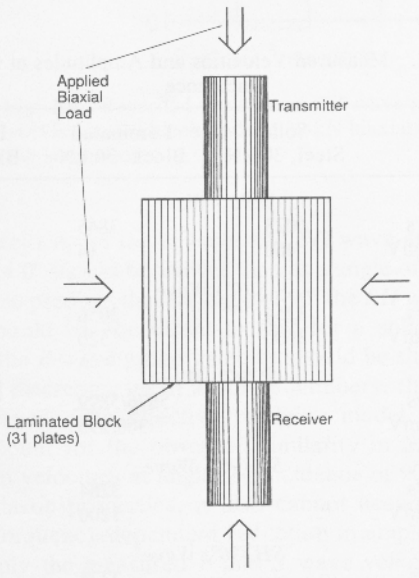

Fig. 11. Sketch of biaxial loading system used to apply load to the laminated block consisting of 31 steel plates.

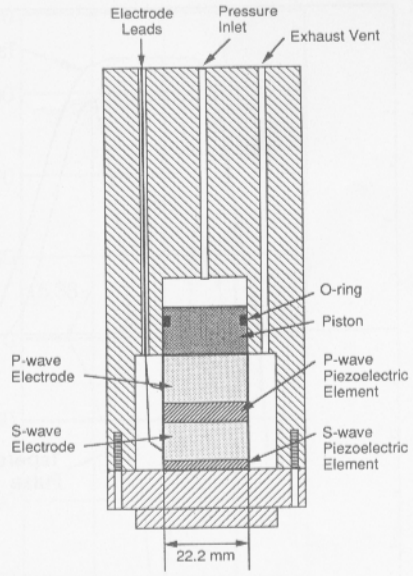

Fig. 12. Sketch of seismic transducer containing piezoelectric elements.

portion of the cylinder in front of the piston containing the elements and electrodes is vented. The nitrogen pressure ensures good seismic coupling between the piezoelectric elements and the end closure in contact with the specimen. The pressure was maintained constant with a regulator.

The natural frequency of each piezoelectric element in the transducers was about 1 MHz, and the transmission crystals were pulsed with a 1 kV spike of 0.3 μs duration at a repetition rate of 100 Hz (Velonex high-power pulse generator, model 350). The receiver elements were terminated with a 50-ohm impedance and dc coupled to a Tektronics (model 7704A) digital oscilloscope. The oscilloscope was triggered by a pulse from the high-voltage pulser through a calibrated variable delay on the oscilloscope so that the arrival time of each pulse could be read to 0.01 μs. Group arrival times were measured for both compressional and shear waves. The oscilloscope was used to digitize and hold a portion of each seismic pulse with a duration of 20 μs. These pulses were digitized (Tektronics P7001 digitizer) at a rate of 25.6 points/μs, and three such digitized pulses were stacked to produce a good signal to noise ratio. The oscilloscope was connected to a PDP 11/44 computer where each record was stored on disc.

To examine the spectral content of the seismic pulse, the received waveform signal was tapered to isolate the initial pulse of the wave from subsequent reflections. Different tapers were evaluated to determine which one would give the best representation of the spectral energy of the first pulse. The selection tapers were found to isolate the initial pulses from the reflections and yet preserve most of the low-frequency content of the signal without too much distortion in the high-frequency range (see, for example, Figure 13). Amplitude spectra were calculated by performing a fast Fourier transform (FFT) on the tapered pulse.

Compressional and shear pulse group travel times and transmitted amplitudes were measured at angles of incidence of 0° (normal to the fractures) and 90° (parallel to the fractures). Two polarizations of one *S* wave were measured when propagating in the direction parallel to the fractures.

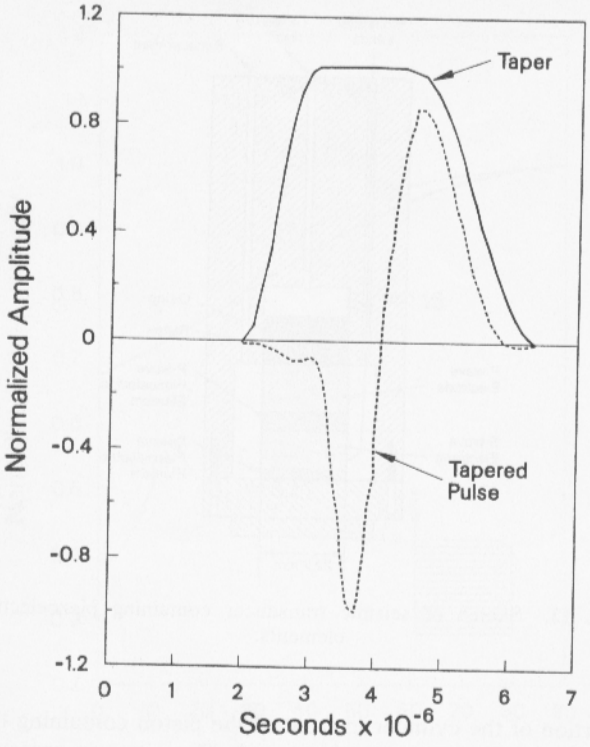

Fig. 13. Taper applied to S wave pulse and a typical waveform resulting from the tapering procedure.

Measurements of group travel time and transmitted wave amplitudes were also made on the solid steel cylinder. Both the laminated block and the solid cylinder were subjected to loads of 15 kN and 30 kN. Good contact between the seismic transducers and the steel blocks was insured by the insertion of a thin lead foil, 25 μm in thickness, between the transducers and the sample.

Experimental Results

Table 2 lists the group velocities and peak-to-peak amplitudes of the first arriving pulses from the solid steel cylinder and the laminated block consisting of 31 steel plates. Peak-to-peak amplitudes were determined from the difference between the trough and the peak amplitudes of the pulse. Data for the laminated steel block are given for biaxial loading conditions of 15 kN and 30 kN for waves propagated at angles of incidence of 0° (perpendicular to the interfaces between plates) and 90° (parallel to interfaces). Two values of group velocity and received pulse amplitude are given for P waves for the 90° incidence for the laminated block corresponding to each orientation of shear wave polarization.

Table 2 shows that the group velocities and peak-to-peak pulse amplitudes of received P and S waves for the 0° direction for the laminated block under a 30-kN load were much lower than those for the solid cylinder or the laminated block at an angle of incidence of 90°. For the 90° angle of incidence in the laminated block the P, SH, and SV wave group velocities approached the value of group velocity from the solid cylinder. Though the group velocities for SH and SV waves were very close in value for this propagation direction, the received pulse amplitude for the SV wave was only about one third that of the SH wave.

Velocities and amplitudes of P and S wave pulses at 0° incidence for the laminated block under a 15-kN biaxial load were lower than those for the block under a 30-kN load. This is consistent with the assumption that the higher load increased the specific stiffness of the interfaces.

Figures 14 and 15 contain the recorded waveforms of P and S wave pulses for the solid cylinder under uniaxial load of 30 kN and the laminated block under a biaxial load of 30 kN. The trends shown by the data in Table 2 can be seen from comparison of the various waveforms. In addition, Figures 14 and 15 also show the variations in frequency content of the waveforms for the various test conditions. Figure 14 shows that the received P wave pulse for the solid cylinder contains higher frequencies than the received pulse for the laminated block at either an angle of incidence of 90° (Figures 14c–14d) or 0° (Figure 14b). As can be seen, the effect was much more pronounced at 0° than at 90°.

Figure 15 contains the waveforms of S wave pulses propagated through the solid cylinder (Figure 15a), the laminated block at 0° incidence (Figure 15b), and the laminated block at 90° incidence for both shear wave polarizations (Figures 15c–15d). For 0° incidence the S wave pulse is not only slower and of much lower amplitude but also has much lower frequency content than any of the other S wave pulses. The waveform of the SV wave pulse incident at 90° (Figure 15d) exhibits both a lower amplitude and a higher frequency content than the SH wave (Figure 15c).

The difference in amplitude and frequency content of the waveforms for the two S wave polarizations at 90° incidence is further illustrated by the spectra of the two waveforms shown in Figure 16. For the SH wave pulse a maximum spectral amplitude of about 62 occurs at about 300 kHz while for the SV wave pulse the maximum spectral amplitude is about 27 at 600 kHz.

Discussion of Experimental Results

The plots in Figures 8, 9, and 10 can be used to show qualitatively the trends that would be expected if the laminated block were represented by a transversely isotropic medium. At angles of incidence of 0° and 90° it is consistent to refer to the $S1$ and $S2$ waves as SH and SV waves, respectively. Thus the effective moduli model predicts that

TABLE 2. Measured Velocities and Amplitudes at 0° and 90° Incidence

	Solid Steel, 30 kN	Laminated Block, 30 kN	Laminated Block, 15 kN
	P (0°) Wave		
Velocity, m/s	6023	3845	3581
Amplitude, mV	460	14	9
	S (0°) Wave		
Velocity, m/s	3254	2056	1702
Amplitude, mV	3600	520	220
	P (90°) Wave		
Velocity, m/s		5876/5899	5815/5838
Amplitude, mV		300/295	68/73
	SV (90°) Wave		
Velocity, m/s		3284	3272
Amplitude, mV		1200	348
	SH (90°) Wave		
Velocity, m/s		3274	3249
Amplitude, mV		4200	960

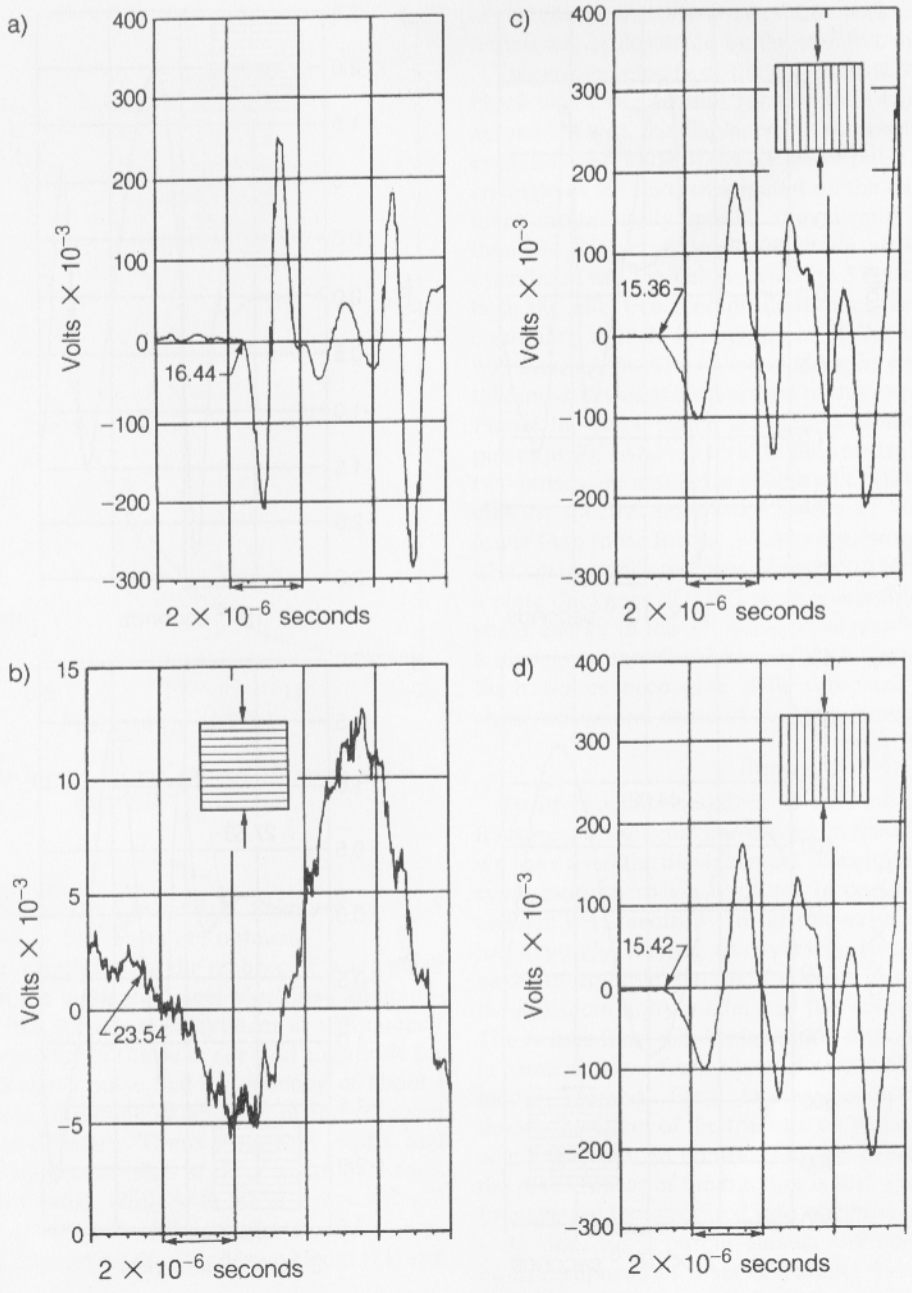

Fig. 14. Recorded waveforms of P wave pulses propagated through (*a*) solid steel cylinder under a 30 kN load and (*b*)–(*d*) laminated block under a 30-kN biaxial load. The insets show the location of the transducer (arrow) with respect to the laminations.

the group velocity of the P wave and SH wave at angles of incidence of 0° should be slower than at a angle of incidence of 90°. It also predicts that an angle of 90° the SH wave group velocity should be equivalent to that for a solid piece of steel, and the P wave group velocity should be slightly less. With small discrepancies in absolute numbers, these trends were observed. The effective modulus model, however, cannot account for the observed similarity in SH and SV wave group velocities at angles of incidence of 90°. Assuming only elastic properties, it also cannot account for the observed frequency-dependent reduction in amplitudes.

Using only the measured P and S wave velocities at an angle of incidence of 0°, the effective moduli model can also be used to estimate quantitatively values of κ_N and κ_T for the interfaces between the steel plates. On the basis of (20) and (21), using travel times under a 30 kN load and the material properties of steel listed in Table 1, values of $\kappa_N = 6 \times 10^{13}$ Pa/m and $\kappa_T = 2 \times 10^{13}$ Pa/m were obtained.

The displacement discontinuity model permits evaluation of the effect of a series of parallel fractures on both velocity and amplitudes. With respect to the laminated steel block tests the displacement discontinuity model would predict that the group velocities of all three waves, P, SH, and SV at 0° incidence should be reduced compared to those for the solid steel block, and at 90° incidence the group velocities of all three waves should approach the values for the solid block (see Figures 3, 4, and 5). The displacement discontinuity model predicts that the amplitude of the transmitted

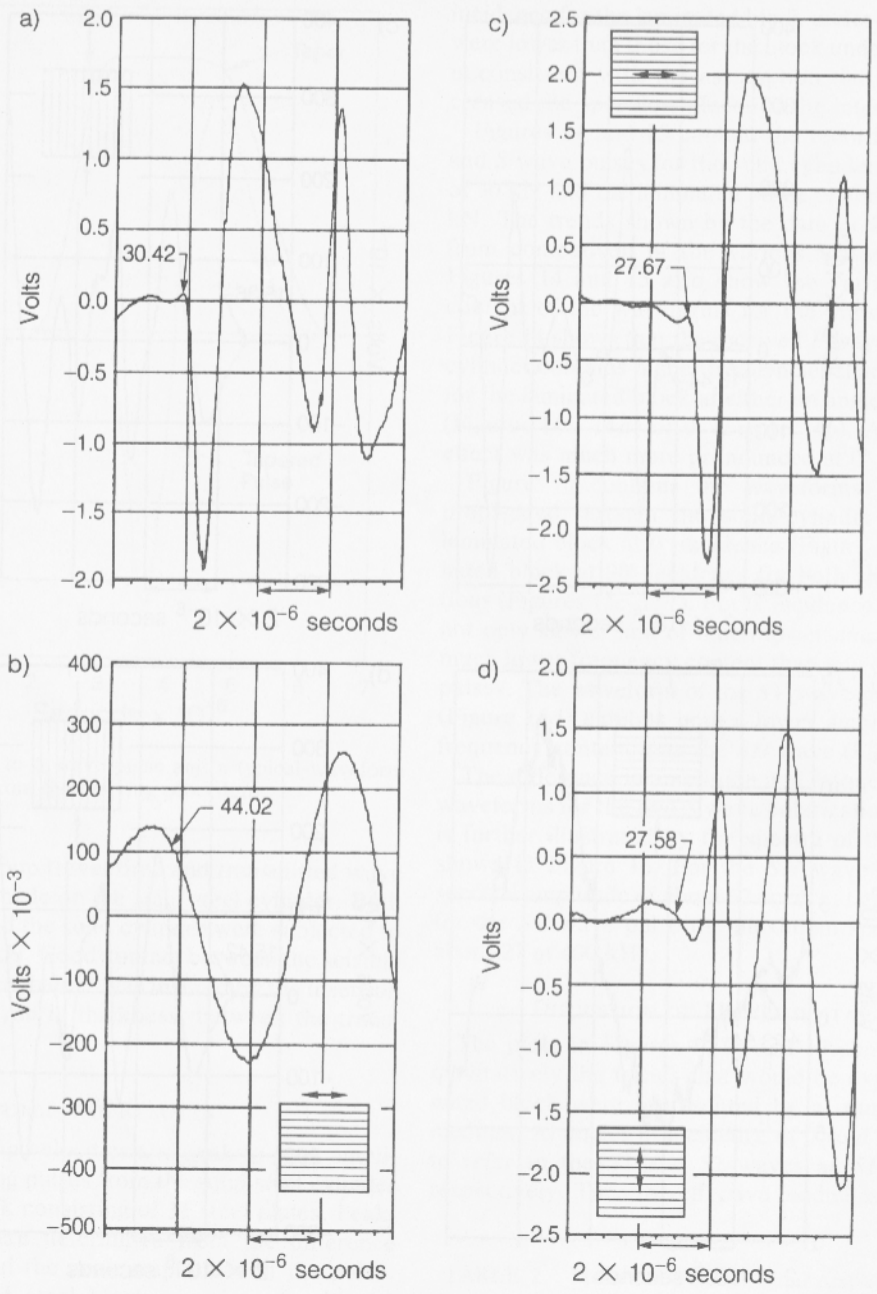

Fig. 15. Recorded waveforms of S wave pulses propagated through (*a*) solid steel cylinder under a 30 kN load and (*b*)–(*d*) laminated block under a 30 kN biaxial load. The insets show the polarization of particle motion with respect to the laminations.

wave will be reduced according to the value of $|T|^{30}$ where $|T|$ is the magnitude of the frequency-dependent transmission coefficient for a wave propagating across one of the 30 interfaces in the laminated block. At 0° incidence the value of $|T|$ is dependent upon the specific stiffness of the interfaces and the frequency of the propagating wave. At 90° incidence the displacement discontinuity model predicts that the group velocities of P and SV waves approach those of intact material, while their amplitudes go to zero (Figure 6). For the SH wave at 90° incidence the displacement discontinuity model predicts that the amplitude will approach that of intact material.

At 0° incidence the observed results corresponded well with predictions of the displacement discontinuity model, that is, the received P and S wave pulses for the laminated block were lower in velocity and much lower in frequency and amplitude than those for the intact cylinder (Figures 14 and 15). On the basis of the displacement discontinuity model the velocities and amplitudes at 0° incidence can be used independently to estimate values of κ_N and κ_T for the interfaces in the laminated block. Using the difference between arrival times for P and S wave pulses in the solid cylinder and in the laminated block at 0° under a 30-kN load, estimates of κ_N and κ_T were obtained using (16). Values of $\omega = 1 \times 10^6$ s^{-1} for P waves and $\omega = 1.1 \times 10^6$ s^{-1} for S waves, which correspond to the center frequency of the received pulse for the laminated block at 0°, were used in the calculation. It is noted that (16) has two roots, so, from the P wave data, values of $\kappa_N = 9.3 \times 10^{13}$ Pa/m and 5.9×10^{12}

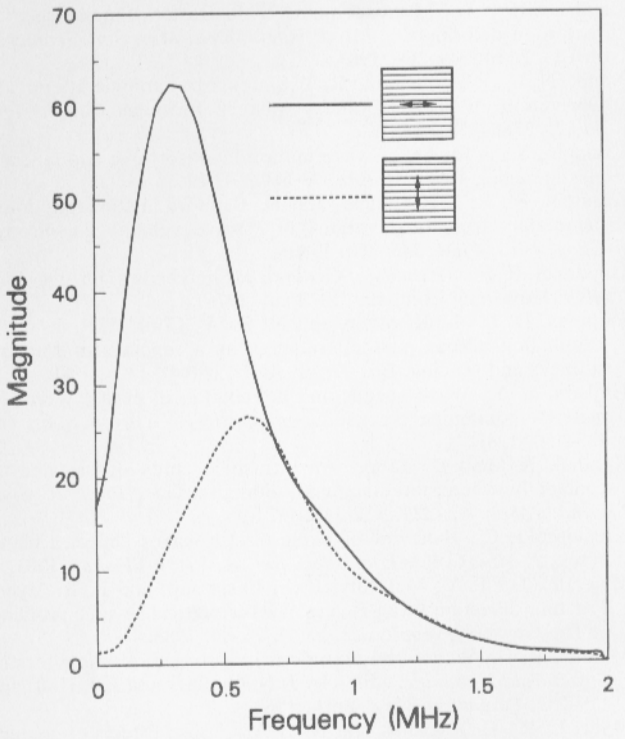

Fig. 16. Shear wave spectra for the *SV* and *SH* wave pulses in Figure 15.

Pa/m are obtained. From the *S* wave data, values of $\kappa_T = 1.5 \times 10^{13}$ Pa/m and 1.3×10^{13} Pa/m are obtained.

The peak spectral amplitude for the received *P* wave pulse propagated through the laminated steel block had an amplitude of about $\frac{1}{10}$ of that for the solid cylinder at a frequency of about $\frac{1}{5}$ of the frequency of the peak spectral amplitude for the cylinder. The *S* wave pulse had a frequency of about $\frac{1}{3}$ and an peak spectral amplitude of about $\frac{1}{10}$ of the received pulse for the solid cylinder. These frequency shifts and amplitude changes suggest a value of $|T|$ of about 0.93 for a single interface. This value, along with the $\omega = 1 \times 10^6$ s^{-1} for *P* waves and $\omega = 1.1 \times 10^6$ s^{-1} for *S* waves, was substituted into the expression for $|T|$ obtained from (13) and given by

$$|T| = \left[\frac{4(\kappa/Z)^2}{4(\kappa/Z)^2 + \omega^2}\right]^{1/2} \tag{24}$$

The solution of this equation yielded one real root each for κ_N and κ_T. These values are $\kappa_N = 5.9 \times 10^{13}$ and $\kappa_T = 3.5 \times 10^{13}$.

At 90° incidence the velocity of the *SH* wave for the laminated block was about equal to that for the intact cylinder, as predicted by either the displacement discontinuity model or the effective moduli model. The amplitude, however, was greater than that observed in the intact cylinder. This result remains unexplained.

The observed group velocity of the *P* wave at 90° incidence was lower than that predicted by displacement discontinuity model. The observed amplitude while lower than for the intact cylinder, was much larger than anticipated on the basis of the displacement discontinuity model. One explanation for the large amplitude of the *P* wave pulse is that none of the energy actually crosses an interface, so that this wave propagates as described by the effective moduli method.

The group velocity of the *SV* wave at 90° in the laminated block was close to that for the solid cylinder, in apparent agreement with the displacement discontinuity model. However, the amplitude of the *SV* wave pulse was also greater at an angle of 90° than anticipated on the basis of the displacement discontinuity model, though still significantly lower than the *SH* wave pulse amplitude at 90° or for the solid cylinder. Thus the behavior of the *SV* wave was contrary to both the effective moduli model and the displacement discontinuity model. It appears as if the laminated structure was filtering out *SV* wave wavelengths greater than the plate thickness. Evidence in support of this explanation is found in Figure 16, which shows the spectra for the *SV* and *SH* waves pulses at 90°. Above 600 kHz the spectral amplitudes for the two pulses are similar in magnitude, while at lower frequencies the spectral amplitudes for the *SV* wave pulse are much lower than those for the *SH* wave pulses. A frequency of 600 kHz corresponds to a wavelength of 0.005 m, compared with a plate thickness of 0.003 m. It is possible that the observed shear energy in the *SV* wave pulse was being propagated as a dispersive interface wave [*Pyrak-Nolte and Cook*, 1987]. Such waves propagate with velocities between those of shear waves and those of Rayleigh waves.

SUMMARY

To investigate the effect of discrete structures, such as fractures, on seismic anisotropy in velocity and amplitudes, we have used the displacement discontinuity model for wave propagation across a fracture. In our analysis we chose to analyze the anisotropy in seismic velocities and amplitudes for a purely elastic, transversely isotropic medium composed of multiple, parallel fractures using both the displacement discontinuity model and the effective moduli method. The results from the displacement discontinuity model differ in several ways from those determined from the effective moduli method. First, in the displacement discontinuity theory the effect of the fracture on wave propagation occurs at the fracture. In contrast, in the effective moduli method the discreteness of the fracture is lost when the effects of the fracture are incorporated into effective moduli.

Second, for a purely elastic, transversely isotropic medium composed of a set of parallel fractures, the displacement discontinuity model predicts a group velocity and a transmitted wave amplitude that depend on the frequency of the wave, the ratio of fracture specific stiffness to seismic impedance, and the angle of incidence. The effective moduli method does not yield frequency-dependent group velocities nor changes in the amplitudes of transmitted waves. Frequency dependence can be introduced into the effective moduli method using complex moduli. However, the medium then is no longer purely elastic, but is viscoelastic.

A third and very important difference is the behavior of the *SV* wave group velocity and transmitted wave amplitude when the wave is propagated parallel to the fractures. The effective moduli method predicts that the *SV* wave group velocity at an angle of incidence of 90° will be equal to the value of *SV* wave and *SH* wave group velocities at 0° incidence (perpendicular to the fractures). On the other hand, the displacement discontinuity model predicts that the group velocity of the *SV* wave at an angle of 90° (parallel to the fractures) will be equal to the group velocity assumed for

the intact portion of the medium. When the waves are propagated parallel to the fracture, the fractures do not cause a delay or phase shift in the wave front, and the wave travels through the intact portions of the medium. This also means that at 90° the group velocities of *P* and *SH* waves propagated parallel to the fracture will equal the group velocity of a wave propagated through intact material.

From the experimental results the dependence of group velocity and wave amplitude on fracture specific stiffness was observed by comparing the results for normal incidence when the block consisting of 31 steel plates was subjected to loads of 15 kN and 30 kN. As the load was increased, the fracture stiffness increased, thereby increasing the group velocity and increasing the transmitted wave amplitude. Increasing the stiffness of the interfaces in the steel laminated block also resulted in an increase in the high-frequency content of the signals. For waves propagated perpendicular to the interfaces, group velocities were reduced compared to the solid steel cylinder in accordance with both the effective moduli model and the displacement discontinuity model. The displacement discontinuity model, however, was able to predict not only the decrease in group velocities but also the reduction in amplitudes and changes in frequency content assuming no additional material parameters. At 90° incidence the transmitted waves did not cross the interfaces. The *P* wave group velocity was closer to that predicted by the effective moduli model than that predicted by the displacement discontinuity model. However, for 90° incidence, neither model could account for the observed velocity of the shear wave with particle motion perpendicular to the fractures. For the particular plate thickness used in the experiment, this direction of propagation seems to act as a high pass filter for *S* wave wavelengths shorter than the spacing between the interfaces.

In conclusion, the displacement discontinuity model for wave propagation through multiple parallel fractures predicts anisotropy in velocity and wave amplitudes that depend on the angle of incidence, on the frequency of the signal, and on the ratio of fracture specific stiffness to the seismic impedance. Though further experimental data are needed to confirm predictions of the displacement discontinuity model at oblique angles of incidence, the difference in behavior of the displacement discontinuity model in comparison with traditional models could result in significantly different interpretations of field data.

Acknowledgments. This work was funded in part by the National Science Foundation under grant EE-830053 and by the Director, Office of Energy Research, Office of Basic Energy Sciences, Division of Engineering, Mathematics and Geosciences, and Assistant Secretary for Nuclear Energy, Office of Civilian Radioactive Waste Management, Division of Siting and Facilities Technology Division, Office of Facilities Siting and Development of the U.S. Department of Energy under contract DE-AC03-76SF00098. We also acknowledge Ivan Psencik of the Czechoslovakian Academy of Sciences Geophysical Institute for his elucidating comments regarding wave propagation in anisotropic media.

REFERENCES

Aki, K., and R. G. Richards, *Quantitative Seismology, Theory and Methods*, vol. 1, pp. 133–144, W. H. Freeman, New York, 1980.

Amadei, B., and R. E. Goodman, A 3-D constitutive relation for fractured rock masses, in *Studies in Applied Mechanics*, part 5B, *Mechanics of Structured Media: International Symposium on the Mechanical Behavior of Structural Media, Ottawa*, pp. 249–268, Elsevier, New York 1981.

Bandis, S. C., A. C. Lumsden, and N. R. Barton, Fundamental of rock joint deformation, *Int. J. Rock Mech. Min. Sci. Geomech. Abstr.*, *20*(6), 249–268, 1983.

Banik, N. C., I. Lerche, and R. T. Shuey, Stratigraphic fittering, I, Derivation of the O'Doherty-Anstery formula, *Geophysics*, *50*(12), 2768–2774, 1985.

Crampin, S., A review of wave motion in anisotropic and cracked elastic media, *Wave Motion*, *3*, 343–391, 1981.

Crampin, S., R. McGoningle, and D. Bamford, Estimating crack parameters from observations of *P*-wave velocity anisotropy, *Geophysics*, *43*(3), 345–360, 1980.

Goodman, R. E., *Methods of Geological Engineering*, pp. 170–173, West Publishing Company, St. Paul, 1976.

Hopkins, D. L., L. R. Myer, and N. G. W. Cook, Seismic wave attenuation across parallel fractures as a function of fracture stiffness and spacing, *Eos Trans. AGU*, *69*(44), 1427, 1988.

Hudson, J. A., Wave speeds and attenuation of elastic waves in material containing cracks, *Geophys. J. R. Astron. Soc.*, *64*, 133–150, 1981.

Kendall, K., and D. Tabor, An ultrasonic study of the area of contact between stationary and sliding surface, *Proc. R. Soc. London, Ser. A*, *1323*, 321–340, 1971.

Kitsunezaki, C., Behavior of plane elastic waves across a plane crack, *J. Min. Coll. Akita Univ., Ser. A*, *VI*(3), 173–187, 1983.

Majer, E. L., T. V. McEvilly, F. S. Eastwood, and L. R. Myer, Fracture detection using *P*- and *S*-wave vertical seismic profiling at The Geysers, *Geophysics*, *53*(1), 76–84, 1988.

Mindlin, R. D., Waves and vibrations in isotropic, elastic plates,in *Structural Mechanics*, edited by J. N. Goodier and J. J. Hoff, pp. 199–232, Pergamon, New York, 1960.

Myer, L. R., D. Hopkins, and N. G. W. Cook, Effects of contact area of an interface on acoustic wave transmission characteristics, in *Research of Engineering Applications in Rock Masses*, vol. 1, edited by E. Ashworth, pp. 565–572, A. A. Balkema, Boston, Mass., 1985.

Pyrak, L. J., Seismic visibility of fractures, Ph.D. thesis, Univ. of Calif., Berkeley, 1988.

Pyrak-Nolte, L. J., and N. G. W. Cook, Elastic interface waves along a fracture, *Geophys. Res. Lett.*, *14*(11), 1107–1110, 1987.

Pyrak-Nolte, L. J., L. R. Myer, and N. G. W. Cook, Seismic visibility of fractures, in *Proceedings of the 28th U.S. Symposium on Rock Mechanics*, edited by I. W. Farmer et al., pp. 47–56, A. A. Balkema, Boston, Mass., 1987.

Raven, K. G., and J. E. Gale, Water flow in natural fractures as a function of stress and sample size, *Int. J. Rock Mech. Min. Sci. Geomech. Abstr.*, *22*, 251, 1985.

Schoenberg, M., Elastic wave behavior across linear slip interfaces, *J. Acoust. Soc. Am.*, *68*(5), 1516, 1980.

Schoenberg, M., Reflection of elastic waves from periodically stratified media with interfacial slip, *Geophys. Prospect.*, *31*, 265–292, 1983.

Schoenberger, M., and F. K. Levin, Apparent attenuation due to interbed multiples, *Geophysics*, *39*(3), 278–291, 1974.

Spencer, T. W., C. M. Edwards, and J. R. Sonnad, Seismic wave attenuation in nonresolvable cyclic stratification, *Geophysics*, *42*(5), 939–949, 1977.

Swan, G., Determination of stiffness and other joint properties from roughness measurements, *Rock Mech. Rock Eng.*, *16*(1), 19–38, 1983.

Thomsen, L., Weak elastic anisotropy, *Geophysics*, *51*(10), 1954–1966, 1986.

White, J. E., *Underground Sound*, pp. 49–53, Elsevier, New York, 1983.

N. G. W. Cook, Department of Materials Science and Mineral Engineering, University of California, Berkeley, CA 94720.

L. R. Myer, Lawrence Berkeley Laboratory, Earth Sciences Division, University of California, 1 Cyclotron Road, Berkeley, CA 94720.

L. J. Pyrak-Nolte, Department of Earth and Atmospheric Sciences, Purdue University, West Lafayette, IN 47907.

(Received February 27, 1989;
revised November 27, 1989;
accepted November 5, 1989.)